THE JOURNAL OF BIOLOGICAL CHEMISTRY VOL. 288, NO. 17, pp. 12042–12053, April 26, 2013

Toward Understanding the Outer Membrane Uptake of Small Molecules by *Pseudomonas aeruginosa*[*] [S]

Received for publication, February 21, 2013, and in revised form, March 5, 2013 Published, JBC Papers in Press, March 6, 2013, DOI 10.1074/jbc.M113.463570

Elif Eren[‡], **Jamie Parkin**[§], **Ayodele Adelanwa**[‡], **Belete Cheneke**[¶], **Liviu Movileanu**[¶], **Syma Khalid**[§1], **and Bert van den Berg**[‡2]

From the [‡]*Program in Molecular Medicine, University of Massachusetts Medical School, Worcester, Massachusetts 01605,* [§]*Systems and Synthetic Biology Modelling Group, School of Chemistry, University of Southampton, Southampton SO17 1BJ, United Kingdom, and the* [¶]*Department of Physics, Syracuse University, Syracuse, New York 13244-1130*

Background: Occ channels mediate small molecule uptake in Pseudomonads.
Results: We have analyzed a number of site-directed mutants for two Occ channels.
Conclusion: Pores of OccD subfamily members are highly flexible. The central basic ladder residues interact with the substrate carboxyl group and are essential for transport.
Significance: The data provide the first atomistic insights into transport by an important class of OM channels.

Because small molecules enter Gram-negative bacteria via outer membrane (OM) channels, understanding OM transport is essential for the rational design of improved and new antibiotics. In the human pathogen *Pseudomonas aeruginosa*, most small molecules are taken up by outer membrane carboxylate channel (Occ) proteins, which can be divided into two distinct subfamilies, OccD and OccK. Here we characterize substrate transport mediated by Occ proteins belonging to both subfamilies. Based on the determination of the OccK2-glucuronate co-crystal structure, we identify the channel residues that are essential for substrate transport. We further show that the pore regions of the channels are rigid in the OccK subfamily and highly dynamic in the OccD subfamily. We also demonstrate that the substrate carboxylate group interacts with central residues of the basic ladder, a row of arginine and lysine residues that leads to and away from the binding site at the channel constriction. Moreover, the importance of the basic ladder residues corresponds to their degree of conservation. Finally, we apply the generated insights by converting the archetype of the entire family, OccD1, from a basic amino acid-specific channel into a channel with a preference for negatively charged amino acids.

Gram-negative bacteria usually have a much higher intrinsic resistance toward antibiotics than Gram-positive bacteria due to the presence of an additional, outer membrane (OM)[3] in Gram-negative bacteria (1). The outer membrane is a unique, asymmetrical bilayer due to the presence of lipopolysaccharide (LPS), a complex glycolipid that makes up the outer leaflet of the OM (1). The presence of LPS is the reason that the OM comprises a very effective barrier against the permeation of both hydrophobic and hydrophilic compounds (1, 2). Because of the effectiveness of the OM, channels are required for diffusion-mediated uptake of small molecules required for cell growth and function. Importantly, most if not all antibiotics that are currently on the market enter Gram-negative bacteria via OM channels (3).

OM diffusion channels can be grouped in two classes based on their interaction with substrates. The first class constitutes porins, which have large channels that allow nonspecific passage of polar molecules smaller than ~600 Da (1). Because porins do not bind their substrates with high affinities, they are efficient when external substrate concentrations are high. The second class of OM diffusion channels constitutes substrate-specific channels. The principal difference between substrate-specific channels and porins is that the pores of the former class are smaller in size, allowing diffusion of only a limited number of compounds (1). Furthermore, substrate-specific channels bind their substrates with higher affinities than porins, making substrate-specific channels effective at low substrate concentrations in the external environment.

Besides being intrinsically resistant toward antibiotics, (Gram-negative) bacteria can acquire antibiotic resistance, and it is this type of resistance that poses an increasingly large problem for the treatment of bacterial infections worldwide (4). The emergence of antibiotic resistance can be caused by bacterium-mediated changes in the interaction of the drug with its target as well as by changes in one or more of the three processes that determine intracellular drug concentrations, *i.e.* uptake, efflux, and enzymatic degradation (3, 4). Regarding uptake, there are many examples in the literature where the emergence of antibiotic resistance is correlated with changes in OM channels at either the DNA level (*e.g.* down-regulation of expression) or protein level (*e.g.* loss-of-function mutations; Refs. 3, 5, and 6). Despite the importance of channels for uptake, it is unclear how antibiotics pass through OM channels with the exception of the

* This work was supported, in whole or in part, by National Institutes of Health Grants R01 GM088403 (to L. M.) and R01 GM085785 (to B. v. d. B.). This work was also supported by National Science Foundation Grant DMR-1006332 (to L. M.).
[S] This article contains a supplemental movie.
The atomic coordinates and structure factors (codes 4FMS and 4FOZ) have been deposited in the Protein Data Bank (http://wwpdb.org/).
[1] Research Councils UK Fellow.
[2] To whom correspondence should be addressed: Inst. for Cellular and Molecular Biosciences, The Medical School, Newcastle University, Newcastle-upon-Tyne NE2 4HH, UK. E-mail: bert.van-den-berg@ncl.ac.uk.
[3] The abbreviations used are: OM, outer membrane; Occ, outer membrane carboxylate channel; MD, molecular dynamics; pS, picosiemens; IM, inner membrane; DMPC, *1,2-dimyristoyl-sn-glycero-3-phosphocholine*.

Escherichia coli porins OmpC/F (7–11). Understanding how antibiotics and other small molecules pass through OM channels should enable the rational design of novel antibiotics with superior permeation properties.

Pseudomonas aeruginosa PAO1 is a paradigm for OM impermeability and antibiotic resistance. It is one of the most notorious Gram-negative pathogens and is responsible for ~10% of hospital-acquired infections (5, 12, 13). *P. aeruginosa* is intrinsically resistant to many antibiotics, which is partly due to a lack of large channel porins such as *E. coli* OmpF/C. Instead of porins, *P. aeruginosa* has approximately 30 substrate-specific channels. Nineteen of those belong to the outer membrane carboxylate channel (Occ) family, making Occ proteins responsible for uptake of the majority of small molecules, including antibiotics, in *P. aeruginosa* (14). The archetype of the family, OccD1 (formerly OprD), is known to be an uptake channel for basic amino acids and clinically important carbapenem antibiotics (15–17). Our recent structural and biochemical characterization of the majority of the Occ protein family has revealed that the two Occ subfamilies (OccD and OccK) have very different substrate specificities. OccD family members transport positively charged amino acids, and OccK proteins have a preference for cyclic compounds with a net negative charge, such as benzoate (18). The requirement of substrates for all family members is that they possess a carboxyl group. Taken together, the data showed how bacteria containing Occ proteins are able to effectively take up a range of substrates while still maintaining a highly effective OM barrier (18).

Despite these advances in understanding Occ-mediated small molecule uptake, it is still unclear which channel residues are important for transport and how those residues interact with substrates. In the present study, we have identified essential residues and clarified their roles for a member of each Occ subfamily by using an integrated approach of x-ray crystallography, biochemical characterization of mutant proteins, and molecular dynamics simulations. We have applied the generated insights by changing the specificity of the archetypal OccD1 protein. The results and applied methodologies do not only shed light on the transport mechanism of Occ proteins but also illustrate part of a general strategy for the design and optimization of more effective antibiotics with enhanced OM permeation properties.

EXPERIMENTAL PROCEDURES

Cloning, Expression, and Purification of OccK2 and OccD1 Mutants—OccK2 and OccD1 eyelet mutations were made with the QuikChange site-directed mutagenesis kit (Stratagene, La Jolla, CA) using OccK2-pB22 and OccD1-pB22 plasmids (18) as DNA templates. Deletion of the OccD1 L7 loop insertion was carried out using overlap extension PCR (19). DNA sequencing was performed at Center for AIDS Research DNA sequencing facility (University of Massachusetts Medical School, Worcester, MA). BL21(DE3) T1 phage-resistant cells (New England Biolabs, Ipswich, MA) were transformed with OccK2 or OccD1 mutant constructs. Expression and purification of (mutant) proteins was done as described previously (18).

TABLE 1
Data collection and refinement statistics of OccK2-glucuronate and OccD1 (Y282R/D307H)

	OccK2-glucuronate	OccD1 (Y282R/D307H)
Data collection		
Beamline	NSLS X6A	NSLS X25
Wavelength	1.10	0.972
Space group	$P2_1$	C2
Cell dimensions		
a, *b*, *c* (Å)	46.4, 206.8, 51.7	148.5, 104.8, 47.4
α, β, γ (°)	90, 99.1, 90	90, 98.6, 90
Resolution (Å)[a]	50-2.45 (2.49-2.45)[a]	50-2.40 (2.44-2.40)
Completeness	89.5 (90.0)	94.4 (97.2)
Redundancy	1.9 (1.8)	4.8 (4.6)
I/σ	14.3 (2.4)	18.0 (1.8)
R_{sym}	5.3 (24.1)	8.4 (71.6)
Refinement		
Resolution (Å)	15-2.45 (2.52-2.45)	15.0-2.4 (2.50-2.40)
Unique reflections[b]	32,300 (1,888)	26,345 (1,318)
R_{work}/R_{free}[c]	19.0/24.2	19.7/23.9
r.m.s.d.[d]		
Bond lengths (Å)	0.008	0.008
Bond angles (°)	1.17	1.10
Atoms		
Protein/glucuronate	5,753/26	2,949/—[e]
Sulfate/detergent/water	20/207/230	—/110/78
B-factors		
Protein/glucuronate	32.2/34.2	47.8/—
Sulfate/detergent/water	54.0/42.8/32.4	—/73.4/46.2
Ramachandran plot favored/allowed/outliers (%)	97.0/3.0/0.0	95.8/4.2/0.0
MolProbity Clashscore	8.9	8.9

[a] Values in parentheses are for the highest resolution shell.
[b] Values in parentheses are the number of reflections used to calculate R_{free}.
[c] $R_{work} = \Sigma|F_o - F_c|/\Sigma F_o$. R_{free} is the cross-validation of the *R*-factor.
[d] Root mean square deviation.
[e] —, not present.

Crystallization of Occ Channels and Structure Determinations—OccK2-glucuronate crystals were obtained by adding 1 μl of 10 mg/ml protein solution to 1 μl of mother liquor containing 25% PEG 1000, 50 mM glucuronate, 50 mM Li_2SO_4, 50 mM Na_2SO_4, and 50 mM sodium acetate, pH 5.5 using hanging drop vapor diffusion. OccD1 Y282R/D307H crystals were obtained by adding 1 μl of 12 mg/ml protein solution to 1 μl of 2.0 M $(NH_4)_2SO_4$, pH 6.0. Diffraction data were collected at 100 K at the National Synchrotron Light Source (Brookhaven National Laboratory) at beamlines X6A and X25. Processing was carried out with HKL2000 (20). The Occ channel structures were solved by molecular replacement in Phaser (21) using OccK2 (Protein Data Bank code 3SZD) and OccD1 (Protein Data Bank code 3SY7) as the search models. Model (re)building was performed manually within Coot (22), and the structures were refined using PHENIX (Table 1) (23). Structure validation was performed within PHENIX.

Radiolabeled Substrate Uptake Assays—Expression of wild type or mutated Occ proteins in BL21 omp8 (Δ*lamB ompF*::Tn*5* Δ*ompA* Δ*ompC*) cells (24) and membrane vesicle preparations were performed as described previously (18). Total membrane vesicles containing overexpressed Occ proteins were diluted to a 1 mg/ml total membrane protein concentration in 10 mM HEPES, pH 7.0 buffer. Uptake experiments were started with the addition of either 1 μl of 50 μM [^{14}C]arginine (PerkinElmer Life Sciences) or 50 μM [^{3}H]glucuronic acid (American Radiolabeled Chemicals, St. Louis, MO) to 100 μl of OccD1 and OccK2 membrane vesicles, respectively. Uptake was carried out at 25 °C for 15 min. Membrane vesicles were

TABLE 2
System compositions and simulation details

System	Protein	Mutation	Substrate	Restraints	Lipids	Solvent	Simulation length
							ns
3SY7-a	3SY7 + modeled loops	No	NA[a]	Yes[b]	170 DMPC	~14,000 H_2O and 15 Na^+	100
3SY7-b	3SY7 + modeled loops	Yes	NA	Yes[b]	170 DMPC	~14,000 H_2O and 12 Na^+	100
3SY7-c	3SY7 + modeled loops	No	Arginine	No	170 DMPC	~14,000 H_2O and 14 Na^+	100
3SY7-d	3SY7 + modeled loops	No	Glutamate	No	170 DMPC	~14,000 H_2O and 16 Na^+	100
3SY7-e	3SY7 + modeled loops	Yes	Arginine	No	170 DMPC	~14,000 H_2O and 11 Na^+	100
3SY7-f	3SY7 + modeled loops	Yes	Glutamate	No	170 DMPC	~14,000 H_2O and 13 Na^+	100

[a] NA, not applicable.
[b] Refers to restraints of 1,000 kJ mol^{-1} nm^{-2} on the β-sheets of the barrel.

filtered using 0.22-μm nitrocellulose filters (Millipore, Billerica, MA) and washed with 3 ml of HEPES buffer. The filters were then placed in scintillation vials containing 5 ml of Econo-Safe scintillation fluid (Atlantic Nuclear Corp., Rockland, MA) and counted using an LS 6500 multipurpose scintillation counter (Beckman Coulter, Brea, CA). Occ protein quantities in membrane vesicles were determined by comparison of the band intensities in Western blots with that of purified OccD1 using the Kodak 1D 3.6 digital imaging program (Eastman Kodak Co.). For quantification of the proteins in the Western blots, the histidine tag was detected using Penta-His HRP conjugate (Qiagen, Germantown, MD). Glutamic acid uptake experiments for mutant OccD1 proteins were carried out as described above by adding 1 μl of 50 μM [^{14}C]glutamic acid (PerkinElmer Life Sciences) to 100 μl of OccD1 vesicles. Uptake was carried out at 25 °C for 15 min.

Single Channel Current Recordings on Planar Lipid Bilayers—Analysis of the single channel conductance of the OccD1 ΔL7 mutant was carried as described previously (18).

Addition of Missing Loop Regions for Molecular Dynamics (MD) Simulations—Loop residues 32–37, 77–94, 160–170, 287–290, and 422–488, which were unresolved in the OccD1 x-ray structure (Protein Data Bank code 3SY7), were added using the MODELLER program (25). The protein structures with added loops were analyzed and validated by measuring the ϕ and ψ backbone dihedral angles using PDBsum (25–27).

Docking Calculations—All docking calculations were performed using AutoDock4.0 through the graphical user interface AutoDockTools 1.5.4 (28–31). A total of 12 unique docking calculations was performed (excluding repeats). The arginine and glutamate substrates were treated as flexible ligands with seven and five rotatable bonds, respectively. Each protein channel structure was treated as a rigid body. A "grid box" large enough to encompass the interior loop regions of the proteins was used; this incorporated a spacing of 0.264 Å and 126, 126, and 96 points in the *x*, *y*, and *z* dimensions (with *z* being perpendicular to the bilayer), respectively. The number of genetic algorithm runs was set to 30, and the maximum number of energy evaluations was set to 25,000,000. The default values were used for the remaining parameters. The arginine and glutamate substrates had charges of +1 and −1, respectively.

Simulation Protocols—All simulations were performed using the GROMACS package (32–34) version 4.5.5, the GROMOS 54A7 force field (35) for the protein and ions, and GROMOS 53A6-Kukol (36) for DMPC lipid molecules and the simple point charge water model (37). The DMPC bilayer, solvent, and protein were kept at 313 K using Nosé-Hoover temperature coupling with a time constant of 0.5 ps (38, 39). A constant pressure of 1 bar was maintained using the Parrinello-Rahman barostat in a semi-isotropic fashion; *i.e.* the *z* axis (perpendicular to the bilayer) is treated independently of the *x* and *y* axes (40, 41). The pressure coupling used a time constant of 0.5 ps. The electrostatic interactions were treated using the smooth particle mesh Ewald (42) algorithm with a short range cutoff of 9 Å. The van der Waals interactions have an upper limit of 14 Å with a long range dispersion correction applied to the energy and pressure. All bonds were constrained using the LINCS algorithm (43) with a time step of 2 fs.

System Compositions—A summary of all the systems simulated is provided in Table 2. The mutated protein structures had the residues Tyr^{176}, Tyr^{282}, and Asp^{307} converted to Arg^{176}, Arg^{282}, and His^{307} using DeepView-Swiss-PdbViewer (44).

Simulation Details—100-ns MD simulations were performed on 3YS7-a and 3SY7-b with position restraints of 1000 kJ mol^{-1} nm^{-2} on the β-sheet of the barrel, allowing equilibration and free movement of the loop regions. The initial configurations of the systems 3SY7-c and 3SY7-d were obtained from the most energetically favorable docking configurations of arginine and glutamate with the equilibrated 3SY7-a. Likewise, the initial configurations of the systems 3SY7-e and 3SY7-f were obtained from the most energetically favorable dockings of arginine and glutamate on the equilibrated 3SY7-b. 3SY7-c, 3SY7-d, 3SY7-e, and 3SY7-f were simulated for 100 ns unrestrained. VMD (45) was used for visual analysis and production of molecular graphical images.

RESULTS

Co-crystal Structure of an Occ Channel Complexed with Substrate—To understand the role of individual residues during substrate transport, a channel-substrate structure is required. We initially focused our efforts on obtaining co-crystal structures for OccD1 and OccK1, the archetypes of the two Occ subfamilies and the first family members for which the three-dimensional structures were determined (46, 47). Extensive co-crystallization efforts and soaking trials with substrates were not successful for these two channels, however. Upon further characterization of the Occ family, it became clear that this was either due to the fact that crystallization favors partially closed states of some channels (OccD1) or that the compounds used were not optimal transport substrates (OccK1 and vanillate; Ref. 18). Our subsequent studies led to the crystallization of seven additional Occ family members and to identification of preferred substrates for the majority of the family (18), increasing the opportunities and likelihood of success for the co-crys-

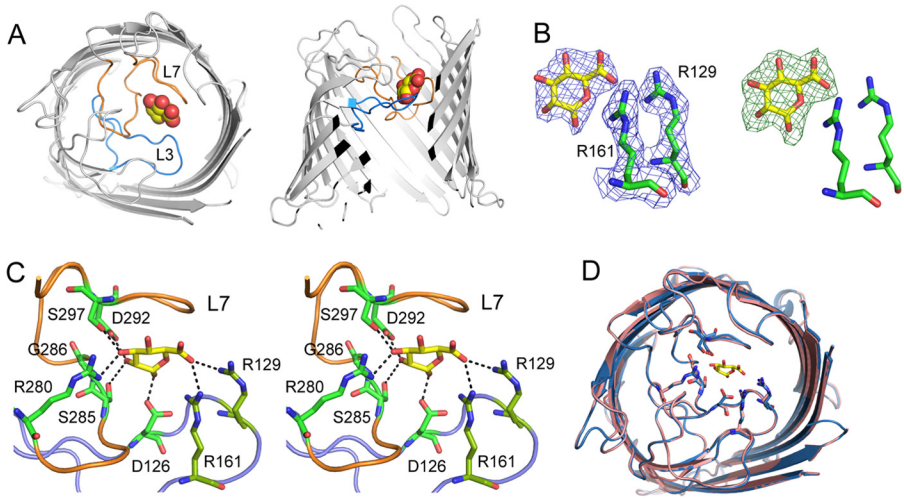

FIGURE 1. **X-ray crystal structure of OccK2 with glucuronate substrate.** *A*, schematic diagram viewed from the top (*left panel*) and from the side (*right panel*) showing the position of the glucuronate molecule as a *space-filling* model (carbons, *yellow*; oxygens, *red*). The pore-constricting loops L3 and L7 are colored *blue* and *orange*, respectively. *B*, $2F_o - F_c$ density (*left panel*) and $F_o - F_c$ density (*right panel*) for the glucuronate molecule and the basic ladder residues Arg^{129} and Arg^{161} contoured at 1.0 σ. *C*, stereodiagram viewed from the extracellular side showing the interaction of glucuronate with eyelet residues of OccK2. Hydrogen bonds are indicated with *dashed lines* (distance, <3.5 Å). Loop L3 is colored *blue*, and loop L7 is colored *orange*. *D*, superposition of apo-OccK2 (Protein Data Bank code 3SZD) and the current Occk2-glucuronate structure. The side chains of residues that interact with glucuronate are shown for both structures. All structural figures were made using PyMOL.

tallization trials. One of the channels, OccK2 (formerly OpdF), crystallized under fairly favorable conditions (pH 5.5 and relatively low ionic strength). *In vitro* transport experiments identified the carboxylic acid sugar glucuronate as a good substrate of this channel (18). Glucuronate is commonly found in glycoproteins and is also part of mucous animal secretions, such as saliva, and may therefore be a physiological substrate of *P. aeruginosa*. We set up crystallization trials of OccK2 with glucuronate, obtained well diffracting crystals, and solved the structure of the channel-substrate complex at 2.45-Å resolution and R_{free} of 24.2% (Fig. 1 and Table 1).

The OccK2-glucuronate structure shows that the substrate is bound at the constriction or "eyelet" of the channel formed by the extracellular loops L3 and L7 and the barrel wall (Fig. 1*A*). That the substrate is observed at this position makes sense because at the constriction the substrate interacts with channel residues from all sides and may therefore bind with the highest affinity. The density for glucuronate is well defined, allowing unambiguous placement of the substrate (Fig. 1*B*). The residues in OccK2 contacting the substrate are Asp^{126} and Arg^{129} in loop L3, Arg^{161} in L4, and Arg^{280}, Ser^{285}, Gly^{286}, Asp^{292}, and Ser^{297} in loop L7. The channel-substrate contacts are exclusively polar and are dominated by hydrogen bonds (Fig. 1*C*). Importantly, ionic interactions are present between the substrate carboxyl group and Arg^{129} and Arg^{161} of the basic ladder (Fig. 1*C*), confirming our prediction that the basic ladder residues interact with the substrate carboxyl group during transport (18, 47). Virtually all OccK2-glucuronate interactions are mediated by side chains of channel residues with only one residue interacting with the substrate via its backbone amide (Gly^{286}). In contrast to other sugar-transporting OM channels of which substrate-bound structures have been solved (*e.g.* LamB; Refs. 48 and 49) there is no "greasy slide"; *i.e.* there are no aromatic residues that interact with the substrate.

An interesting property of many Occ proteins, including OccK2, is their dynamic behavior in single channel conductance experiments (18, 50, 51). Although the conductance of the most dominant state of OccK2 is relatively large for a substrate-specific channel (~230 pS in 1 M KCl), there are frequent downward conductance spikes that occasionally close the channel completely (18). Given this behavior of the channel, the question of whether or not substrate binding and transport require conformational changes in the channel becomes important. A superposition of apo-OccK2 and OccK2-glucuronate clearly shows that both structures are virtually identical (Fig. 1*D*). This observation suggests that at least for OccK2 conformational changes are not required during substrate binding and transport.

Functional Characterization of OccK2 and OccD1 Eyelet Mutants—Based on the OccK2-glucuronate structure, we made site-directed alanine mutants of the eyelet residues that interact with the substrate and assayed *in vitro* radiolabeled glucuronate uptake by total membrane vesicles (18). The results reveal that transport is very sensitive to mutation. Most of the residues that interact with the substrate give a complete loss of transport when mutated to alanine (Fig. 2*A*). The two exceptions are the S285A and S297A mutants, which still show reasonable levels of transport (75 and 35% of wild type OccK2, respectively). The mild effect of the S285A mutation on transport can be explained by the structure, which suggests that the geometry of the serine and substrate hydroxyl groups is not optimal for formation of a hydrogen bond.

Our recent structural and functional characterization of Occ family members revealed that the OccD and OccK subfamilies are quite distinct despite having similar folds (18). In the crystal structures, the pores of OccK channels are all wide enough to transport their substrates as exemplified by the OccK2-glucuronate system (Fig. 1). By contrast, the OccD proteins have very narrow or closed pores that most likely correspond to (partially) closed channels. On a functional level, the substrate specificities between the two subfamilies are also very different with OccD family members transporting linear substrates with a net

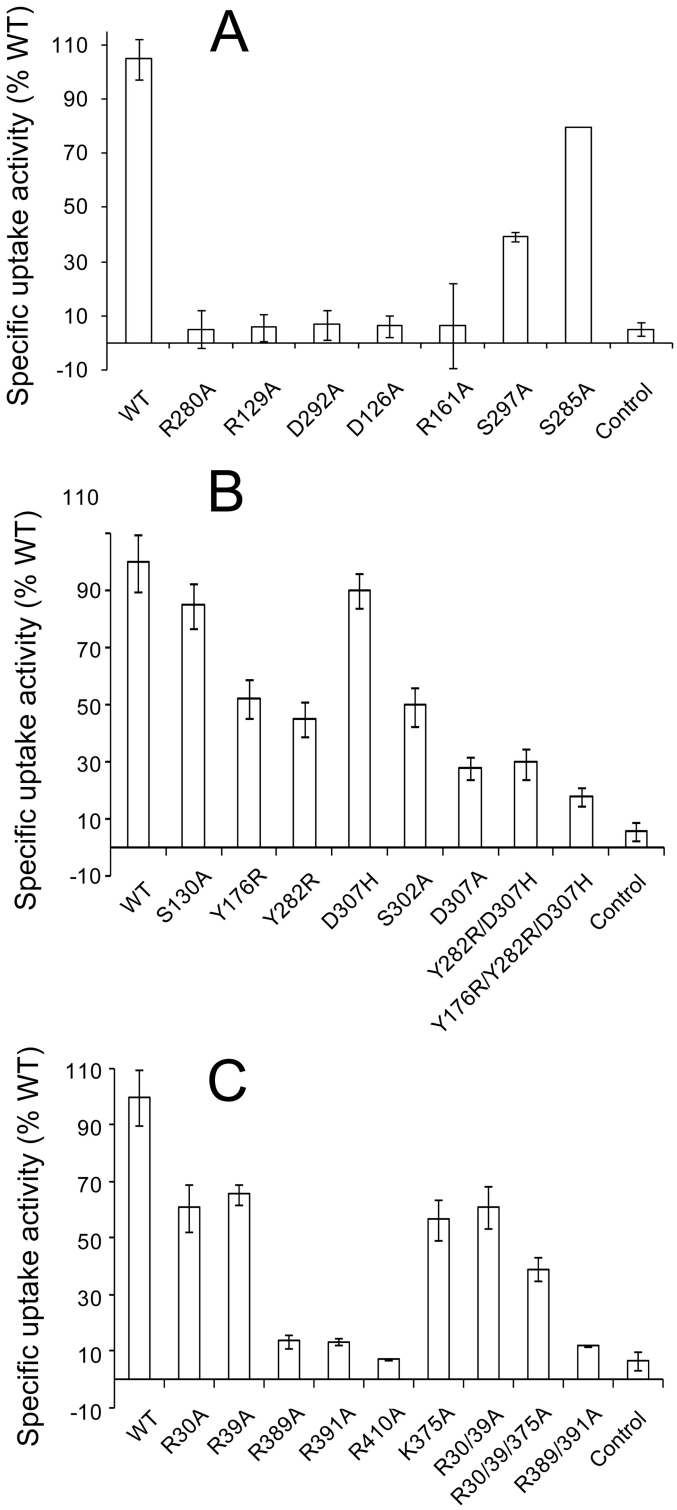

FIGURE 2. **Effect of eyelet residue mutations on transport by OccK and OccD family members.** *A*, characterization of radiolabeled glucuronate uptake by OccK2 mutant proteins. *B* and *C*, characterization of radiolabeled arginine uptake by OccD1 proteins with mutations in the eyelet (*B*) and in the basic ladder (*C*). Uptake activities are shown as a percentage of WT and are specific uptake activities. *Control*, cells transformed with empty plasmid. *Error bars* represent S.D.

positive charge and OccK proteins preferring cyclic substrates with a net negative charge (18). Because of these differences, we therefore also set out to characterize the effect of eyelet mutations on transport mediated by the archetype of the OccD subfamily, OccD1 (formerly OprD). Given that an OccD1-substrate structure is not yet available, we identified candidate residues for mutation by overlaying the apo-OccD1 structure with that of OccK2-glucuronate. Based on this analysis, OccD1 has only three eyelet residues with side chains pointing inward and that therefore could interact with substrates (Fig. 3). Single mutations of each of these residues (Ser^{130}, Ser^{302}, and His^{307}) to alanine showed that only the D307A mutant affected arginine uptake by OccD1 substantially (~30% of wild type (WT); Fig. 2*B*).

We previously proposed that arginine binds in the OccD1 eyelet with the carboxyl group close to the central basic ladder residues and with the side chain guanidinium group bound on the opposite side of the eyelet in a negatively charged pocket formed by the side chains of Tyr^{176}, Tyr^{282}, and Asp^{307} (47). This notion is supported by the superposition of OccD1 with the OccK2-glucuronate structure that shows that the distal part of the substrate (relative to the carboxyl group) is close to the negatively charged pocket (Fig. 3). To assess the effect of this pocket on arginine transport, we substituted the tyrosine residues with arginines (Y176R and Y282R) and the aspartic acid with histidine (D307H). The rationale for these mutations was to make the pocket positively charged, possibly interfering with arginine transport. As shown in Fig. 2*B*, each of the individual mutations does not have a large effect on arginine uptake. However, arginine uptake levels of the double mutant (Y282R/D307H) and in particular of the triple mutant (Y176R/Y282R/D307H) are substantially lower and at ~20% of WT levels (Fig. 2*B*). These data indicate that the conversion of the negatively charged pocket to a positively charged pocket is detrimental to arginine transport, supporting the notion that the negatively charged pocket of wild type OccD1 interacts with the positively charged head group of the substrate during transport.

An interesting region near the OccD1 eyelet is the ~8-residue-long insertion in loop L7 (L7i; residues Phe^{285}–Gly^{294}). This region, which is only present in a few OccD family members, partially blocks the pore in the recently determined high resolution structure of OccD1 (Fig. 3 and Ref. 18). We therefore asked whether this insertion is important for arginine uptake. We deleted the L7i segment and replaced it with a glycine residue to have a minimal amount of distortion within the mutant protein. Interestingly, the resulting ΔL7 mutant has almost 2-fold higher arginine uptake than wild type OccD1 (Fig. 4*A*), demonstrating that removal of the pore-blocking segment improves transport. Analysis of the single channel conductance of the ΔL7 mutant showed an ~3-fold increase of conductance relative to wild type OccD1, consistent with a bigger pore being present in the mutant. The single channel electrophysiological signature of the ΔL7 mutant has large upward spikes in conductance (to ~400 pS; Fig. 4, *B* and *C*). Such spikes, which likely correspond to the open channel, are also observed in wild type OccD1 albeit ~10 times less frequently. The fact that the dominant state of the deletion mutant still has a relatively low conductance (~55 pS) suggests that the regions of the structure that are involved in generating an open channel are more extensive than the pore-blocking L7 segment alone.

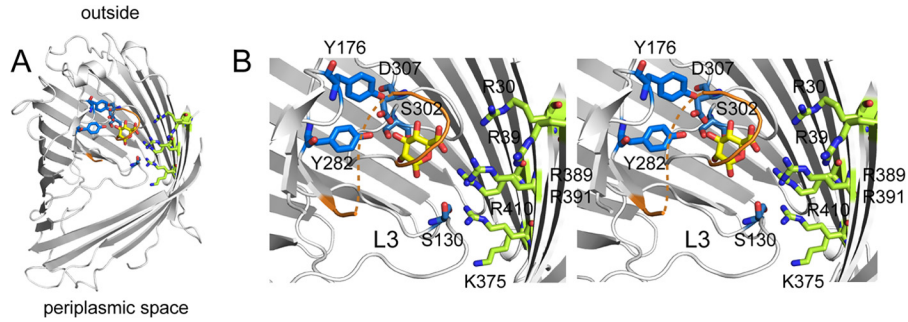

FIGURE 3. **Identification of putative substrate-interacting residues in OccD1.** *A*, overview of a superposition of OccK2-glucuronate and OccD1 (Protein Data Bank code 3SY7). For clarity, the OccK2 protein has been omitted. *B*, close-up stereodiagram showing OccD1 residues that may be important for substrate transport as *stick* models (carbons, *blue*; oxygens, *red*; nitrogens, *dark blue*). The carbon atoms of the basic ladder residues are colored *green*. The insertion of loop L7 that partially blocks the OccD1 pore is colored *orange* with the segment that is disordered shown as a *dashed line* (residues 286–295).

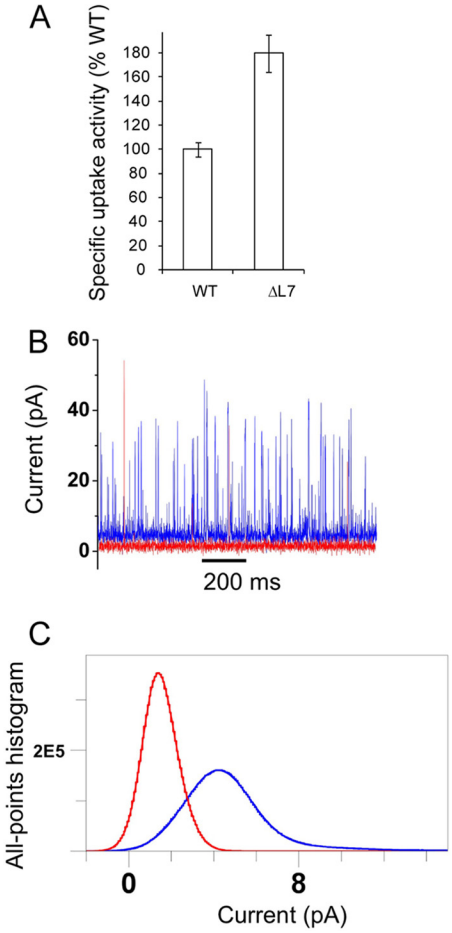

FIGURE 4. **Biochemical and biophysical characterization of the ΔL7 OccD1 mutant protein.** *A*, specific radiolabeled arginine uptake activities. *Error bars* represent S.D. *B*, representative single channel electrical recordings acquired with wild type OccD1 (*red*) and the ΔL7 mutant (*blue*) at a transmembrane potential of +80 mV. The corresponding all-point histograms are shown in *C*. The results of the Gaussian fits of the current amplitudes (conductance values) of wild type OccD1 and its mutant ΔL7 are 1.4 pA (18 pS) and 4.3 pA (54 pS), respectively. For the sake of clarity, the single channel electrical traces were low pass Bessel filtered at 1 kHz. The buffer solution contained 1 M KCl and 10 mM HEPES, pH 7.4.

The Importance of the Basic Ladder Residues for Transport Correlates with Their Degree of Conservation—Our previous, family-wide structural characterization of Occ family members showed that the numbers of basic ladder residues in the various channels range from three to eight (18). Only the three basic ladder residues that are closest to the eyelets of the channels are present in all Occ family members. For OccD1, these residues are Arg^{389}, Arg^{391}, and Arg^{410} (Fig. 3). The lack of conservation for basic ladder residues that are further away from the eyelet (Arg^{30}, Arg^{39}, and Lys^{375} in OccD1; Fig. 3) suggests that they might be dispensable for substrate transport. To test this notion, we determined the arginine uptake activities for all six individual basic ladder mutant proteins of OccD1. The results clearly show that the peripheral ladder residues are non-essential because even the triple mutant (R30A/R39A/K375A) still transports arginine at levels of ~40% of wild type (Fig. 2*C*). By contrast, removal of any one of the central basic ladder residues leads to severe defects in substrate transport (Fig. 2*C*). We conclude that only the central, conserved basic ladder residues are required for efficient substrate uptake in Occ proteins.

Conversion of OccD1 into a Glutamate-preferring Channel—As a yardstick to assess our understanding of substrate uptake by OccD1, we asked whether any of the OccD1 mutant proteins described in the previous section could have a different substrate specificity compared with the wild type protein. We were particularly interested in the mutants that we made for the negatively charged pocket. Replacement of those residues (Tyr^{176}, Tyr^{282}, and Asp^{307}) with positively charged residues decreased arginine uptake in a triple mutant ~5-fold relative to wild type (Fig. 2*B*). Given the likely involvement of the negatively charged pocket in binding the positively charged side chain of the substrate, we reasoned that the positively charged binding pocket mutants might convert the mutant OccD1 protein from a basic amino acid-preferring channel into an acidic amino acid-preferring channel. To test this hypothesis, we assayed the uptake of radiolabeled glutamate by wild type OccD1, the double mutant Y282R/D307H, and the triple mutant Y176R/Y282R/D307H. As expected and consistent with previous measurements (18), wild type OccD1 does not take up glutamate (Fig. 5). Remarkably, both the double and the triple mutants show substantial levels of glutamate uptake with the triple mutant transporting glutamate substantially better than arginine. The change in preference of glutamate over arginine for the triple mutant is more than 400-fold compared with wild type OccD1 (Fig. 5). The ΔL7 mutant, like wild type, does not transport glutamate at significant levels, suggesting that res-

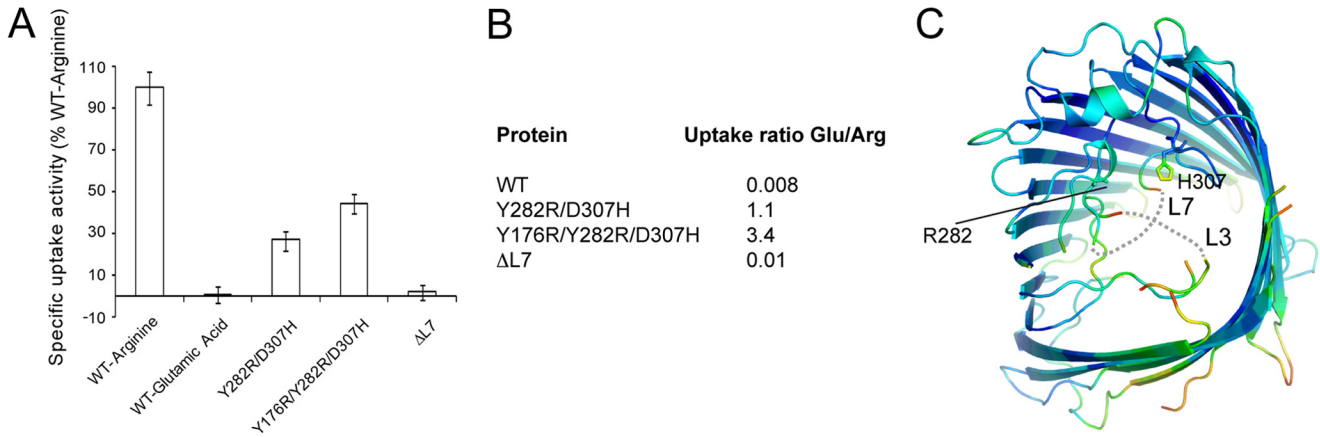

FIGURE 5. **Conversion of the arginine-specific channel OccD1 into a channel preferring acidic amino acids.** *A*, specific radiolabeled glutamate uptake activities of OccD1 mutant proteins with altered substrate headgroup binding. Activities are normalized to arginine uptake by wild type OccD1, which is also shown. *Error bars* represent S.D. *B*, glutamate/arginine uptake ratios for OccD1 mutants. *C*, x-ray crystal structure of the OccD1 double mutant Y282R/D307H. The schematic representation colored by B-factors (*blue*, low B-factor; *red*, high B-factor) shows the disorder in loops L3 and L7. Missing segments are shown as *dashed lines*. The mutated residues Arg^{282} and His^{307} are shown as *stick* models and have been labeled.

idues within the L7 loop insertion do not play a role in the generation of substrate specificity.

To obtain a detailed structural understanding underlying the changes in substrate specificity, we attempted to crystallize the triple OccD1 mutant, but we were not successful. However, we were able to solve the structure of the double OccD1 mutant Y282R/D307H at a resolution of 2.4 Å (Table 1). The structure of this mutant, which also has considerable glutamate transport activity, is characterized by an increase in mobility of the eyelet region (Fig. 5*C*) possibly as a result of the introduced mutations. Electron density for residues 127–130 in loop L3 and residues 286–296 in loop L7 is completely missing. In addition, side chain density for the introduced arginine residue (Arg^{282}) is missing. The structure of the double mutant therefore does not allow us to rationalize the change in its substrate specificity relative to wild type OccD1.

Docking Studies and Molecular Dynamics Simulations Support the Experimental Data—Realistically, experimental structural data of channel-substrate complexes will be obtained for only a limited number of systems. For this reason, MD simulations have a crucial role to play in our understanding of the interactions between uptake channels and small molecules. In addition, MD simulations can provide detailed atomistic-level information about mutant structures and transport intermediates that are not accessible to experimental approaches (52). Here, we asked whether the observed substrate preferences of wild type OccD1 and the triple mutant (Y176R/Y282R/D307H) protein could be understood by performing MD simulations. As the first step, we docked arginine and glutamate into wild type OccD1. A number of independent docking calculations were performed for each case (see "Experimental Procedures"). The results show that the arginine substrate binds at a well defined position close to the eyelet region in wild type OccD1 (Fig. 6). By contrast, the binding of glutamate within wild type OccD1 is poorly defined compared with arginine, and in many docking trials, the glutamate ends up a considerable distance away from the eyelet region (Fig. 6). In addition to wild type OccD1, we also performed docking calculations for arginine and glutamate within the triple mutant Y176R/Y282R/D307H.

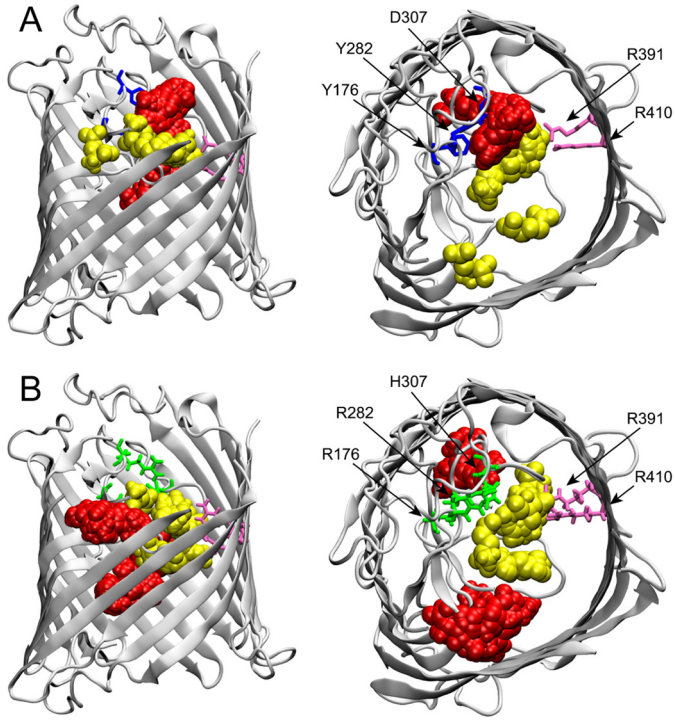

FIGURE 6. **Docking calculations support biochemical transport data.** Views of the 30 lowest free energy of binding conformations of arginine and glutamate substrates after docking to wild type OccD1 (*A*) and the triple mutant Y176R/Y282R/D307H (*B*) are shown. Views are shown from the side (*left panels*) and from the top (*right panels*). The arginine substrates are shown as *space-filling* models in *red*, and the glutamate substrates are shown in *yellow*. In *blue stick* models are shown the residues Tyr^{176}, Tyr^{282}, and Asp^{307} of wild type OccD1. In *green* are the corresponding residues in the triple mutant Arg^{176}, Arg^{282}, and His^{307}. The two central basic ladder residues Arg^{391} and Arg^{410} are shown in *mauve*.

Encouragingly, the docking results for the mutant show a trend opposite to those of the wild type; arginine binds in a poorly defined manner at sites that are not close to the eyelet. In contrast, glutamate binds reproducibly within the eyelet region (Fig. 6). Thus, the docking results are consistent with the substrate preferences of wild type OccD1 and the triple mutant for arginine and glutamate, respectively.

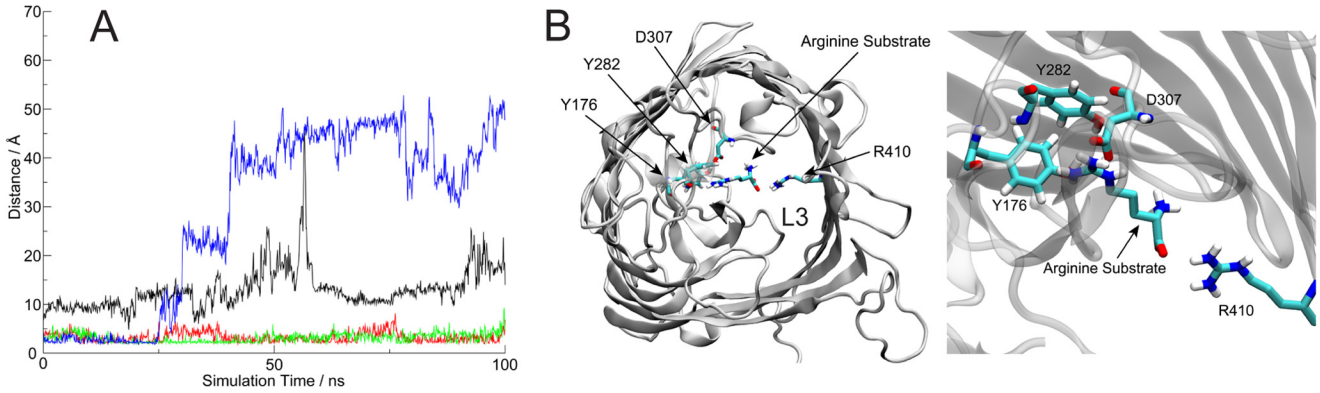

FIGURE 7. **Molecular dynamics simulations of substrates in wild type OccD1 and the triple OccD1 mutant.** *A*, distances of arginine and glutamate substrates from the central basic ladder residue Arg^{410} during 100 ns of simulation (*red*, wild type OccD1-arginine; *blue*, wild type OccD1-glutamate; *green*, mutant OccD1-glutamate; *black*, mutant OccD1-arginine). *B*, overview (*left panel*) and close-up (*right panel*) of the structure of wild type OccD1 with arginine substrate after 100-ns simulation. Arg^{410}, Tyr^{176}, Tyr^{282}, and Asp^{307} are labeled and colored with nitrogens in *blue*, oxygens in *red*, and hydrogens in *white*.

Although the docking studies show relatively well defined binding sites for arginine in wild type OccD1 and for glutamate in the triple mutant, there are two distinct binding clusters for the substrate in both of these cases. One of these clusters corresponds to the binding mode we presume to be correct, *i.e.* with the (main chain) carboxyl close to the basic ladder. Within the other cluster, the side chain interacts with the basic ladder. The docking calculations allow the identification of clusters of favorable binding sites and provide a rational starting point for further computational investigation, but they do not include the effect of solvent or full protein dynamics. We therefore complemented the docking studies by performing 100-ns MD simulations for each of the four different OccD1-substrate combinations (WT-arginine, WT-glutamate, triple mutant-arginine, and triple mutant-glutamate), starting in each case from the lowest energy docking simulations (see "Experimental Procedures"). Previously, a similar MD approach was used to study phosphate binding to *P. aeruginosa* OprP, a phosphate channel that is not related to the Occ family (53). During the OccD1 wild type-arginine simulation, the carboxyl group initially faces away from Arg^{410} in the basic ladder. Subsequently, the arginine molecule flips rapidly to form the predicted interactions of the carboxyl group with Arg^{410} (Fig. 7 and supplemental movie). During the remainder of the simulation, this orientation dominates. At the end of the simulation (t = 100 ns), the arginine is bound in the eyelet as proposed previously with the guanidinium group close to the side chains of Tyr^{176}, Tyr^{282}, and Asp^{307} (Fig. 7*B*). Other residues that interact prominently with the arginine molecule during the simulation are Ser^{130}, Thr^{175}, Ala^{292}/Gly^{294}/Ser^{296} (L7 insertion), and Val^{303}/Qln^{304}/Asp^{307} (L7). For the WT-glutamate simulation, a dramatically different behavior is observed. Although the carboxylate group is initially close to Arg^{410}, the substrate moves rapidly away from the eyelet and is expelled from the channel. Thus, glutamate is not stably bound in wild type OccD1 in accord with the biochemical data. For the triple mutant, the simulations are also in good agreement with the experimental data with only glutamate (and not arginine) remaining bound in the eyelet during the simulation (Fig. 7*A*).

Molecular Dynamics Simulations Reveal That the OccD1 Pore Is Dynamic—Besides supporting our biochemical data, the MD simulations also provide valuable information about OccD1 channel dynamics in particular with respect to the eyelet. To quantify the conformational changes in the eyelet region, the fluctuations in the geometry of this region as defined by inter-residue distances Gln^{296}-Arg^{410} and Gln^{304}-Ser^{130} (Fig. 8) were measured from our 100-ns trajectory of wild type OccD1 with arginine substrate. The Gln^{304}-Ser^{130} distance fluctuated between 5.2 and 9.9 Å. This fluctuation is largely a consequence of the Ser^{130} side chain, which flips between two hydrogen-bonded states; it is either engaged in hydrogen bonding to the arginine substrate or to the nearby Asp^{295}. The Gln^{296}-Arg^{410} distance fluctuated between 4.5 and 10.0 Å, indicating a substantial narrowing of the eyelet (Fig. 8). The conformational change of the channel is a consequence of movement of loop L7, in particular residues 286–295 corresponding to the L7 insertion (Figs. 9 and 10). After ~ 25 ns, the L7 loop residue Arg^{287} was observed to "flip" from initially being hydrogen-bonded to Asn^{358} in loop L8 to a second conformation in which it was lying planar to Tyr^{173} while engaging in hydrogen bonding with Gly^{178} (Fig. 9). This flipping of Arg^{287} was accompanied by a larger conformational rearrangement of L7 in which the loop was observed to "twist" in a manner that prevented further interaction of Arg^{287} with loop L8. The distance between the center of mass of Arg^{287} and residues 353–360 of loop L8 changes by ~ 3 Å during the rearrangement of the flexible L7 loop region. Another indicator of the conformational flexibility within loop L7 is the distance between Ser^{290} in loop L7 and Glu^{403} in loop L9. These residues are normally quite far (~10 Å) apart, but they interact briefly during the 100-ns simulation (Fig. 10). Together, these conformational changes result in a highly variable pore size for OccD1 in accord with the structural and biophysical data.

DISCUSSION

We previously identified glucuronate as a preferred substrate for the OccK2 channel (18), and this has resulted in the first channel-substrate structure of an Occ protein in the present study. The substrate is bound in the eyelet and is contacted on

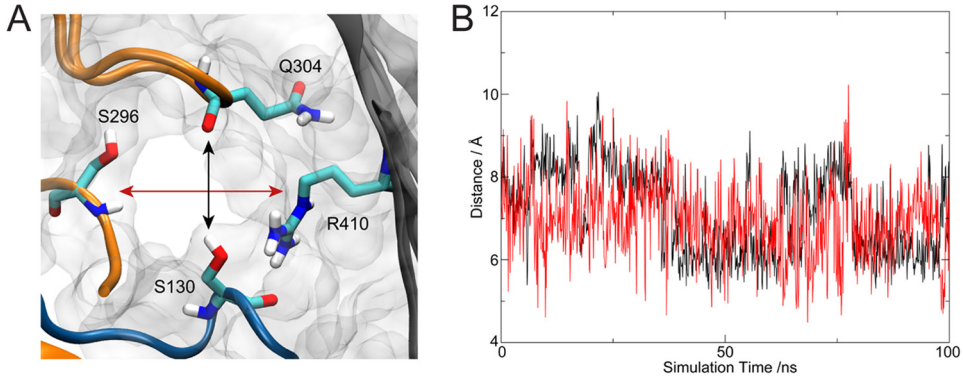

FIGURE 8. **The eyelet diameter of OccD1 is variable.** *A*, top view showing the distances measured to capture the dimensions of the channel at the eyelet. Loop L7 is shown in *orange*, loop L3 is shown in *blue*, and the surface of the protein is shown in *gray*. *B*, minimum distance between OccD1 residues in the eyelet over the course of a 100-ns simulation with an arginine substrate. The minimum distance between Arg^{410} and Ser^{296} is shown in *red*. The minimum distance between Gln^{304} and Ser^{130} is shown in *black*.

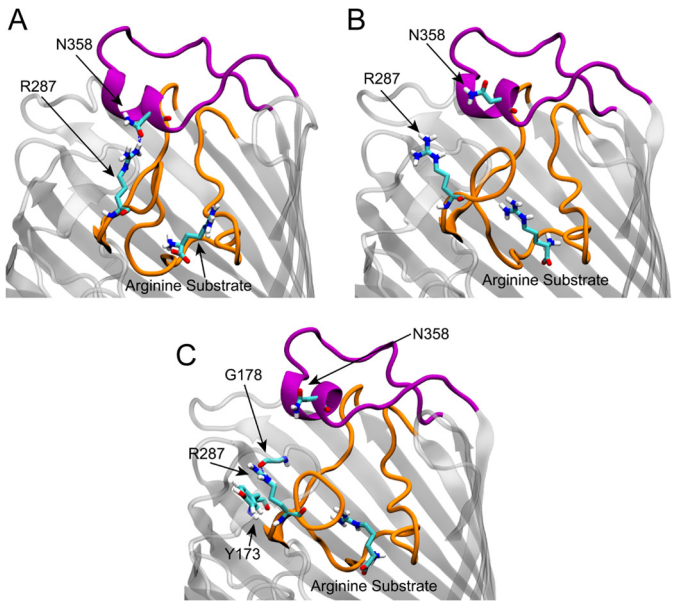

FIGURE 9. **Conformational changes in loop L7 of OccD1 revealed by MD simulation.** *A–C*, snapshots taken at 8, 64, and 64.7 ns, respectively, of the 100-ns MD simulation of wild type OccD1 with arginine substrate. The protein is shown in *gray* with loop L7 colored *orange* and loop L8 colored *purple*. Residues of interest are shown as *stick* models and labeled.

all sides by residues in loops L3 and L7. The carboxylate group of the substrate interacts with the central basic ladder residues in the barrel wall, confirming previous predictions (47).

OccD and OccK Subfamily Proteins Differ in Eyelet Dynamics—Our previous studies suggested indirectly that the eyelets of OccD and OccK subfamily members might be fundamentally different with respect to their dynamics. Our new work confirms this notion. For OccK2, the virtual structural identity of the eyelets in the apo- and substrate-bound structures together with the fact that all OccK proteins have open channels (18) suggests that conformational changes are likely not required for substrate transport by OccK subfamily members. This notion might imply that the current fluctuations observed in single channel experiments (18) result from movement of loop sections that are not part of the eyelets. The relatively static nature of the eyelets should make molecular dynamics simulations of OccK channel-substrate complexes fairly straightforward given the constraint that the carboxyl group of the substrate is close to the central basic ladder residues.

In contrast to OccK proteins, which form relatively rigid channels, OccD family members are much more dynamic. This can be inferred from available structures of OccD proteins (OccD1–3), which all suggest that conformational changes have to occur to allow passage of substrates (18). In addition, our molecular dynamics simulations of OccD1 clearly demonstrate the conformational flexibility of the eyelet region. It is especially noteworthy that the simulations show the frequent formation of a relatively large channel that would likely allow passage of carbapenem antibiotics with a molecular mass of 300–450 Da. The difference in eyelet dynamics between the two Occ subfamilies could explain why mutations of eyelet residues generally have modest effects on OccD1-mediated transport with the exception of the central basic ladder residues (Fig. 2). This contrasts with OccK2 where almost all mutations of residues that interact with the substrate abolish transport (Fig. 2). The data therefore emphasize the remarkable differences between OccD and OccK subfamily members.

Although the apo structures of OccD proteins may not be identical to those of substrate-bound channels, we show that it is still possible to obtain plausible models for substrate translocation without having experimental structural models. This notion is supported by our rational conversion of OccD1 from a channel transporting exclusively positively charged amino acids (arginine) into a channel that prefers negatively charged amino acids (glutamate). The changes in substrate preference resulting from the introduced mutations are supported by docking studies and MD simulations, confirming that computational approaches will have an important role to play in understanding OM channel-substrate interactions at the atomic level. These results are also noteworthy from the point of view of drug design: if it is possible to affect substrate passage by making changes in the channel, it should also be feasible to improve substrate/antibiotic permeation by introducing changes in the substrate/antibiotic.

Implications for Antibiotic Design—Currently, antibiotics directed against pathogenic bacteria are designed for optimal interaction with their target protein inside the cell. Although screening for desirable activities of drug candidates is often straightforward, many compounds having good activity toward

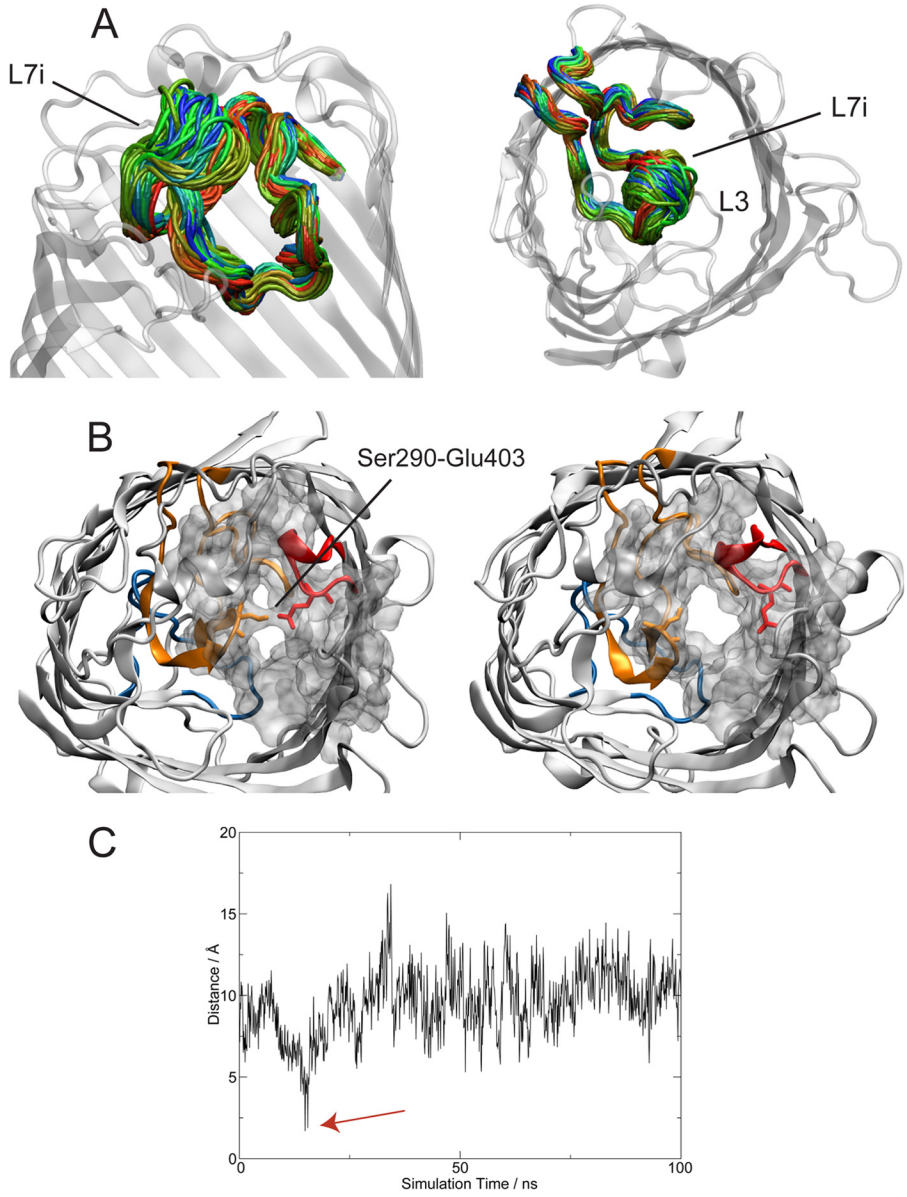

FIGURE 10. **Conformational fluctuations in loop L7 generate large variations in OccD1 pore size.** *A*, views from the side (*left panel*) and from the top (*right p*) showing the fluctuations in loop L7 over the 100-ns simulation. The fluctuations are represented on an RGB scale with *red* at the start of the simulation (0 ns) and *blue* at the end (100 ns). *B*, views from the top showing a small OccD1 pore at 15 ns (*left panel*) and a more typical, open pore at 71 ns (*right panel*). A transient interaction between Ser^{290} in loop L7 and Glu^{403} is highlighted in the *left panel*. Loop L3 is colored *blue*, loop L7 is *orange*, and loop L9 is *red*. For clarity, the arginine substrate has been omitted. *C*, plot showing the minimum distance between Ser^{290} in loop L7 and Glu^{403} in loop L9 during a 100-ns simulation of wild type OccD1 with arginine. The interaction occurring at ~15 ns and that closes the channel briefly is indicated with an *arrow*.

Gram-negative bacteria *in vitro* are poorly effective (or not at all) *in vivo*; *i.e.* minimal inhibitory concentration values are high. The reason for this discrepancy, which is a huge problem in drug development, is that the drug concentrations inside the bacteria are low due to the net outcome of drug uptake, efflux, and degradation. Of these intrinsic resistance factors, intracellular degradation of drugs is relatively well understood and to some extent preventable by modification of the compound (54, 55). By contrast, much less is known about bacterial drug uptake and efflux. Regarding drug efflux, which is mediated by several different families of multidrug efflux pumps, our understanding has greatly increased in recent years by many biochemical and structural studies (56–58). The component of intrinsic resistance that is still very poorly understood is antibiotic uptake. It is generally accepted that the OM forms the biggest barrier for permeation. This is somewhat counterintuitive because the inner membrane (IM) is less permeable than the OM and implies that antibiotics may diffuse spontaneously across the IM due to their partially hydrophobic character. However, it is unclear whether spontaneous diffusion across the IM is sufficient for all antibiotics, and it seems possible (or even likely) that the uptake of some compounds will require IM transporters. To our knowledge, however, no IM transporter has yet been linked to antibiotic uptake. By contrast, there are many examples in the literature about the importance of OM channels for antibiotic uptake. In particular, the emergence of antibiotic resistance in clinical isolates often results from lower levels of functional channels within the OM caused by various

mechanisms (59). With the notable exception of antibiotic transport mediated by the *E. coli* porins OmpF and OmpC (10, 11), however, nothing is known about the molecular mechanisms of antibiotic translocation in OM channels. Moreover, because porins are very different from substrate-specific channels, insights obtained for porin-mediated drug uptake by *E. coli* and other Enterobacteriaceae may not apply to pathogens such as *P. aeruginosa* and *Acinetobacter baumannii*. Thus, studies focused on understanding small molecule uptake in organisms other than *E. coli* are important.

Our present and previous work on Occ channels has generated an understanding of how small molecules interact at the atomic level with OM channels of *P. aeruginosa*. These studies are the first steps toward understanding how antibiotics enter *P. aeruginosa* that in turn could lead to the rational design of new and improved antibiotics. Achieving this goal will require identification of the channels that are important for the pathogen during infection, *e.g.* by using global phenotypic profiling methods for *P. aeruginosa* using an animal model for the cystic fibrosis lung. The rationale behind this is that it makes little sense to design antibiotics to permeate through channels that are not used by the organism during infection or that are easily dispensable. In fact, the well known acquired resistance of *P. aeruginosa* toward carbapenems by down-regulation or deletion of OccD1 suggests the validity of this hypothesis: although we have shown that arginine uptake is mediated by a number of OccD proteins, only OccD1 takes up carbapenem antibiotics (18). Thus, by shutting down OccD1 expression and switching to *e.g.* OccD2, resistance is acquired toward carbapenems without loss of fitness (assuming that arginine is an important food source). We therefore propose a dual strategy in which the identification of important or essential channels *in vivo* is coupled to studying the interaction of small molecules and antibiotics with those channels by biochemical, biophysical, and computational methods. Understanding the basic biology of OM transport could lead to the improvement of existing antibiotic scaffolds and in the longer term to the development of novel, more effective antimicrobial agents that are characterized by optimal permeation properties as well as by being recalcitrant to expulsion from the cell by multidrug efflux pumps.

Acknowledgments—We thank the staff of National Synchrotron Light Source beamlines X6A and X25 for beam time and valuable assistance during data collection. J. P. and S. K. acknowledge use of the Southampton supercomputer, Iridis III.

REFERENCES

1. Nikaido, H. (2003) Molecular basis of bacterial outer membrane permeability revisited. *Microbiol. Mol. Biol. Rev.* **67,** 593–656
2. van den Berg, B. (2010) Going forward laterally: transmembrane passage of hydrophobic molecules through protein channel walls. *Chembiochem* **11,** 1339–1343
3. Pagès, J. M., James, C. E., and Winterhalter, M. (2008) The porin and the permeating antibiotic: a selective diffusion barrier in Gram-negative bacteria. *Nat. Rev. Microbiol.* **6,** 893–903
4. Bolla, J. M., Alibert-Franco, S., Handzlik, J., Chevalier, J., Mahamoud, A., Boyer, G., Kieć-Kononowicz, K., and Pagès, J. M. (2011) Strategies for bypassing the membrane barrier in multidrug resistant Gram-negative bacteria. *FEBS Lett.* **585,** 1682–1690
5. Lister, P. D., Wolter, D. J., and Hanson, N. D. (2009) Antibacterial-resistant *Pseudomonas aeruginosa*: clinical impact and complex regulation of chromosomally encoded resistance mechanisms. *Clin. Microbiol. Rev.* **22,** 582–610
6. Vila, J., Martí, S., and Sánchez-Céspedes, J. (2007) Porins, efflux pumps and multidrug resistance in *Acinetobacter baumannii*. *J. Antimicrob. Chemother.* **59,** 1210–1215
7. Lou, H., Chen, M., Black, S. S., Bushell, S. R., Ceccarelli, M., Mach, T., Beis, K., Low, A. S., Bamford, V. A., Booth, I. R., Bayley, H., and Naismith, J. H. (2011) Altered antibiotic transport in OmpC mutants isolated from a series of clinical strains of multi-drug resistant E. coli. *PLoS One* **6,** e25825
8. Mahendran, K. R., Kreir, M., Weingart, H., Fertig, N., and Winterhalter, M. (2010) Permeation of antibiotics through *Escherichia coli* OmpF and OmpC porins: screening for influx on a single-molecule level. *J. Biomol. Screen.* **15,** 302–307
9. Nestorovich, E. M., Danelon, C., Winterhalter, M., and Bezrukov, S. M. (2002) Designed to penetrate: time-resolved interaction of single antibiotic molecules with bacterial pores. *Proc. Natl. Acad. Sci. U.S.A.* **99,** 9789–9794
10. Kumar, A., Hajjar, E., Ruggerone, P., and Ceccarelli, M. (2010) Structural and dynamical properties of the porins OmpF and OmpC: insights from molecular simulations. *J. Phys. Condens. Matter* **22,** 454125
11. Ziervogel, B. K., and Roux, B. (2013) The binding of antibiotics in OmpF porin. *Structure* **21,** 76–87
12. Breidenstein, E. B., de la Fuente-Núñez, C., and Hancock, R. E. (2011) *Pseudomonas aeruginosa*: all roads lead to resistance. *Trends Microbiol.* **19,** 419–426
13. Mesaros, N., Nordmann, P., Plésiat, P., Roussel-Delvallez, M., Van Eldere, J., Glupczynski, Y., Van Laethem, Y., Jacobs, F., Lebecque, P., Malfroot, A., Tulkens, P. M., and Van Bambeke, F. (2007) *Pseudomonas aeruginosa*: resistance and therapeutic options at the turn of the new millennium. *Clin. Microbiol. Infect.* **13,** 560–578
14. Tamber, S., Ochs, M. M., and Hancock, R. E. (2006) Role of the novel OprD family of porins in nutrient uptake in *Pseudomonas aeruginosa*. *J. Bacteriol.* **188,** 45–54
15. Fukuoka, T., Masuda, N., Takenouchi, T., Sekine, N., Iijima, M., and Ohya, S. (1991) Increase in susceptibility of *Pseudomonas aeruginosa* to carbapenem antibiotics in low-amino-acid media. *Antimicrob. Agents Chemother.* **35,** 529–532
16. Huang, H., and Hancock, R. E. (1996) The role of specific surface loop regions in determining the function of the imipenem-specific pore protein OprD of *Pseudomonas aeruginosa*. *J. Bacteriol.* **178,** 3085–3090
17. Trias, J., and Nikaido, H. (1990) Outer membrane protein D2 catalyzes facilitated diffusion of carbapenems and penems through the outer membrane of *Pseudomonas aeruginosa*. *Antimicrob. Agents Chemother.* **34,** 52–57
18. Eren, E., Vijayaraghavan, J., Liu, J., Cheneke, B. R., Touw, D. S., Lepore, B. W., Indic, M., Movileanu, L., and van den Berg, B. (2012) Substrate specificity within a family of outer membrane carboxylate channels. *PLoS Biol.* **10,** e1001242
19. Heckman, K. L., and Pease, L. R. (2007) Gene splicing and mutagenesis by PCR-driven overlap extension. *Nat. Protoc.* **2,** 924–932
20. Otwinowski, Z., and Minor, W. (1997) Processing of x-ray diffraction data collected in oscillation mode. *Methods Enzymol.* **276,** 307–326
21. Storoni, L. C., McCoy, A. J., and Read, R. J. (2004) Likelihood-enhanced fast rotation functions. *Acta Crystallogr. D Biol. Crystallogr.* **60,** 432–438
22. Emsley, P., and Cowtan, K. (2004) Coot: model-building tools for molecular graphics. *Acta Crystallogr. D Biol. Crystallogr.* **60,** 2126–2132
23. Adams, P. D., Grosse-Kunstleve, R. W., Hung, L. W., Ioerger, T. R., McCoy, A. J., Moriarty, N. W., Read, R. J., Sacchettini, J. C., Sauter, N. K., and Terwilliger, T. C. (2002) PHENIX: building new software for automated crystallographic structure determination. *Acta Crystallogr. D Biol. Crystallogr.* **58,** 1948–1954
24. Prilipov, A., Phale, P. S., Van Gelder, P., Rosenbusch, J. P., and Koebnik, R. (1998) Coupling site-directed mutagenesis with high-level expression: large scale production of mutant porins from *E. coli*. *FEMS Microbiol. Lett.* **163,** 65–72
25. Eswar, N., Webb, B., Marti-Renom, M. A., Madhusudhan, M. S., Eramian,

D., Shen, M. Y., Pieper, U., and Sali, A. (2007) Comparative protein structure modeling using MODELLER. *Curr. Protoc. Protein Sci.* **Chapter 2,** Unit 2.9
26. Laskowski, R. A. (2001) PDBsum: summaries and analyses of PDB structures. *Nucleic Acids Res.* **29,** 221–222
27. Laskowski, R. A., Hutchinson, E. G., Michie, A. D., Wallace, A. C., Jones, M. L., and Thornton, J. M. (1997) PDBsum: a web-based database of summaries and analyses of all PDB structures. *Trends Biochem. Sci.* **22,** 488–490
28. Goodsell, D. S., and Olson, A. J. (1990) Automated docking of substrates to proteins by simulated annealing. *Proteins* **8,** 195–202
29. Huey, R., Morris, G. M., Olson, A. J., and Goodsell, D. S. (2007) A semiempirical free energy force field with charge-based desolvation. *J. Comput. Chem.* **28,** 1145–1152
30. Morris, G. M., Goodsell, D. S., Halliday, R. S., Huey, R., Hart, W. E., Belew, R. K., and Olson, A. J. (1998) Automated docking using a Lamarckian genetic algorithm and empirical binding free energy function. *J. Comput. Chem.* **19,** 1639–1662
31. Morris, G. M., Goodsell, D. S., Huey, R., and Olson, A. J. (1996) Distributed automated docking of flexible ligands to proteins: parallel applications of AutoDock 2.4. *J. Comput. Aided Mol. Des.* **10,** 293–304
32. Berendsen, H. J. C., Vanderspoel, D., and Vandrunen, R. (1995) Gromacs: a message-passing parallel molecular-dynamics implementation. *Comput. Phys. Commun.* **91,** 43–56
33. Hess, B., Kutzner, C., Van Der Spoel, D., and Lindahl, E. (2008) GROMACS 4: algorithms for highly efficient, load-balanced, and scalable molecular simulation. *J. Chem. Theory Comput.* **4,** 435–447
34. Van Der Spoel, D., Lindahl, E., Hess, B., Groenhof, G., Mark, A. E., and Berendsen, H. J. (2005) GROMACS: fast, flexible, and free. *J. Comput. Chem.* **26,** 1701–1718
35. Schmid, N., Eichenberger, A. P., Choutko, A., Riniker, S., Winger, M., Mark, A. E., and van Gunsteren, W. F. (2011) Definition and testing of the GROMOS force-field versions 54A7 and 54B7. *Eur. Biophys. J.* **40,** 843–856
36. Kukol, A. (2009) Lipid models for united-atom molecular dynamics simulations of proteins. *J. Chem. Theory Comput.* **5,** 615–626
37. Berendsen, H. J., Postma, J. P., Van Gunsteren, W. F., and Hermans, J. (1981) Interaction models for water in relation to protein hydration. *Intermol. Forces* **11,** 331–338
38. Hoover, W. G. (1985) Canonical dynamics: equilibrium phase-space distributions. *Phys. Rev. A* **31,** 1695–1697
39. Nosé, S. (1984) A unified formulation of the constant temperature molecular dynamics methods. *J. Chem. Phys.* **81,** 511–519
40. Nosé, S., and Klein, M. L. (1983) Constant pressure molecular dynamics for molecular systems. *Mol. Phys.* **50,** 1055–1076
41. Parrinello, M., and Rahman, A. (1981) Polymorphic transitions in single crystals: a new molecular dynamics method. *J. Appl. Phys.* **52,** 7182–7190
42. Essmann, U., Perera, L., Berkowitz, M. L., Darden, T., Lee, H., and Pedersen, L. G. (1995) A smooth particle mesh Ewald method. *J. Chem. Phys.* **103,** 8577–8593
43. Hess, B. (2008) P-LINCS: a parallel linear constraint solver for molecular simulation. *J. Chem. Theory Comput.* **4,** 116–122
44. Guex, N., and Peitsch, M. C. (1997) SWISS-MODEL and the Swiss-Pdb-Viewer: an environment for comparative protein modeling. *Electrophoresis* **18,** 2714–2723
45. Humphrey, W., Dalke, A., and Schulten, K. (1996) VMD: visual molecular dynamics. *J. Mol. Graph.* **14,** 33–38
46. Biswas, S., Mohammad, M. M., Movileanu, L., and van den Berg, B. (2008) Crystal structure of the outer membrane protein OpdK from *Pseudomonas aeruginosa*. *Structure* **16,** 1027–1035
47. Biswas, S., Mohammad, M. M., Patel, D. R., Movileanu, L., and van den Berg, B. (2007) Structural insight into OprD substrate specificity. *Nat. Struct. Mol. Biol.* **14,** 1108–1109
48. Dutzler, R., Wang, Y. F., Rizkallah, P., Rosenbusch, J. P., Schirmer, T. (1996) Crystal structures of various maltooligosaccharides bound to maltoporin reveal a specific sugar translocation pathway. *Structure* **4,** 127–134
49. Wang, Y. F., Dutzler, R., Rizkallah, P. J., Rosenbusch, J. P., and Schirmer, T. (1997) Channel specificity: structural basis for sugar discrimination and differential flux rates in maltoporin. *J. Mol. Biol.* **272,** 56–63
50. Cheneke, B. R., van den Berg, B., and Movileanu, L. (2011) Analysis of gating transitions among the three major open states of the OpdK channel. *Biochemistry* **50,** 4987–4997
51. Liu, J., Eren, E., Vijayaraghavan, J., Cheneke, B. R., Indic, M., van den Berg, B., and Movileanu, L. (2012) OccK channels from *Pseudomonas aeruginosa* exhibit diverse single-channel electrical signatures but conserved anion selectivity. *Biochemistry* **51,** 2319–2330
52. Khalid, S., Bond, P. J., Carpenter, T., and Sansom, M. S. (2008) OmpA: gating and dynamics via molecular dynamics simulations. *Biochim. Biophys. Acta* **1778,** 1871–1880
53. Pongprayoon, P., Beckstein, O., Wee, C. L., and Sansom, M. S. (2009) Simulations of anion transport through OprP reveal the molecular basis for high affinity and selectivity for phosphate. *Proc. Natl. Acad. Sci. U.S.A.* **106,** 21614–21618
54. Bou, G., Santillana, E., Sheri, A., Beceiro, A., Sampson, J. M., Kalp, M., Bethel, C. R., Distler, A. M., Drawz, S. M., Pagadala, S. R., van den Akker, F., Bonomo, R. A., Romero, A., and Buynak, J. D. (2010) Design, synthesis, and crystal structures of 6-alkylidene-2′-substituted penicillanic acid sulfones as potent inhibitors of *Acinetobacter baumannii* OXA-24 carbapenemase. *J. Am. Chem. Soc.* **132,** 13320–13331
55. Goo, K. S., and Sim, T. S. (2011) Designing new β-lactams: implications from their targets, resistance factors and synthesizing enzymes. *Curr. Comput. Aided. Drug Des.* **7,** 53–80
56. Nikaido, H., and Pagès, J. M. (2012) Broad-specificity efflux pumps and their role in multidrug resistance of Gram-negative bacteria. *FEMS Microbiol. Rev.* **36,** 340–363
57. Nikaido, H., and Takatsuka, Y. (2009) Mechanisms of RND multidrug efflux pumps. *Biochim. Biophys. Acta* **1794,** 769–781
58. Symmons, M. F., Bokma, E., Koronakis, E., Hughes, C., and Koronakis, V. (2009) The assembled structure of a complete tripartite bacterial multidrug efflux pump. *Proc. Natl. Acad. Sci. U.S.A.* **106,** 7173–7178
59. Delcour, A. H. (2009) Outer membrane permeability and antibiotic resistance. *Biochim. Biophys. Acta* **1794,** 808–816